Optical Atomic Switch utilizing a Molecular Junction

Risako Hamase[a], Kanji Homma[a], Tomoaki Nishino[a], Kazuhito Tsukagoshi[b], and Satoshi Kaneko*[c]

a. Department of Chemistry, School of Science, Institute of Science Tokyo, 2-12-1, Ookayama, Meguro-ku, Tokyo 152-8550, Japan

b. International Center for Materials Nanoarchitectonics (MANA), National Institute for Materials Science (NIMS), 1-1 Tsukuba, Ibaraki 305-0044, Japan

c. Department of Materials and Chemical Science, School of Materials and Chemical Technology, Institute of Science Tokyo, 2-12-1 Ookayama, Meguro-ku, Tokyo 152-8550, Japan

†Supplementary Information available:

details of any supplementary information available should be included. DOI: https://doi.org/10.1039/D5TC03002A

Abstract

Optical atomic switches have attracted considerable interest due to its fast switching speed, low energy consumption, and compatibility with quantum information technologies. Although atomic modulation via optical excitation has been demonstrated using scanning probe techniques, controlling atomic motion in operational devices remains a significant challenge for practical applications. In this study, we operated an optical atomic switch and examined the impact of molecular effects on conductance modulation. Single-molecule junctions incorporating C60, bipyridine, and butanediamine were fabricated using a mechanically controllable break junction technique. Photoirradiation induced conductance enhancement in all molecular junctions. Analysis of current–voltage characteristics in ON and OFF states revealed that atomic motion modulates the electronic coupling between the molecule and electrodes. A systematic comparison across different molecular junctions showed that molecular rigidity significantly influences optical conductance modulation, with flexible molecules like butanediamine exhibiting weaker dependence on initial conductance states.

Optical atomic switches have attracted considerable interest due to their rapid switching speed, low energy consumption, and compatibility with quantum information technologies.[1-4] Miniaturization of these devices is expected to further reduce energy demands.[4, 5] Integration with quantum phenomena enables direct interfacing with quantum memory systems, enhancing their versatility in information processing.[6, 7] Furthermore, compatibility with recently proposed synaptic nanodevices positions the atomic optical switch as a promising candidate for in-sensor computing applications.[8, 9] Advances in the optical manipulation of atoms and molecular species have been driven by the development of optical trapping techniques based on laser radiation pressure.[10] Optical tweezers have been successfully used to trap viruses and bacteria.[11, 12] Additionally, near-field effects generated by localized surface plasmon resonance (LSPR) at metallic nanostructures have enabled the trapping of diverse targets, including nanoparticles, biomolecules, and DNA.[13, 14] Zhang et al. demonstrated conductance switching in metallic point contacts under photoirradiation, where plasmonic local heating induces thermal expansion of Au electrodes, leading to the formation of quantum atomic contacts.[3] Electron transport is thus controlled by atomic motion at the nanoscale, triggered by light exposure. These findings highlight the need for further development and multi functionalization of optical atomic switches. Integrating molecular functionalities is expected to enhance both the versatility and performance of these switches.[15, 16] In single-molecule junction (SMJ), hybridization of the molecular and metallic electronic states exhibit unique quantum phenomena, including the Kondo effect,[17] quantum interference,[18] and Fano resonance.[19] However, despite growing interest in hybrids of molecular components and optical switches, the influence of molecular species on atomic motion within optical switches remains

largely unexplored.

Here, this study investigates the molecular influences on atomic motion in optical atomic switches. An SMJ incorporating C_{60}—a promising candidate in molecular electronics[20, 21]—was fabricated using lithographically defined nanoelectrodes.[15, 16, 22] The junction conductance was modulated by near-infrared laser irradiation. Current–voltage (*I*–*V*) analysis revealed that photoirradiation controls the coupling between molecular orbitals and metal electronic states by varying the metal–molecule separation. The observed conductance enhancement is attributed to atomic motion induced by local plasmonic heating. We systematically examined the optical response as a function of conductance, revealing its molecule-dependent behavior. Compared with SMJs based on bipyridine (BPY) and butanediamine (BDA), conductance enhancement under photoirradiation was suppressed in C_{60} and BPY junctions, while BDA showed negligible conductance dependence. Notably, the C_{60}-based optical atomic switch demonstrated stable, repeatable operation at frequencies up to 20 Hz.

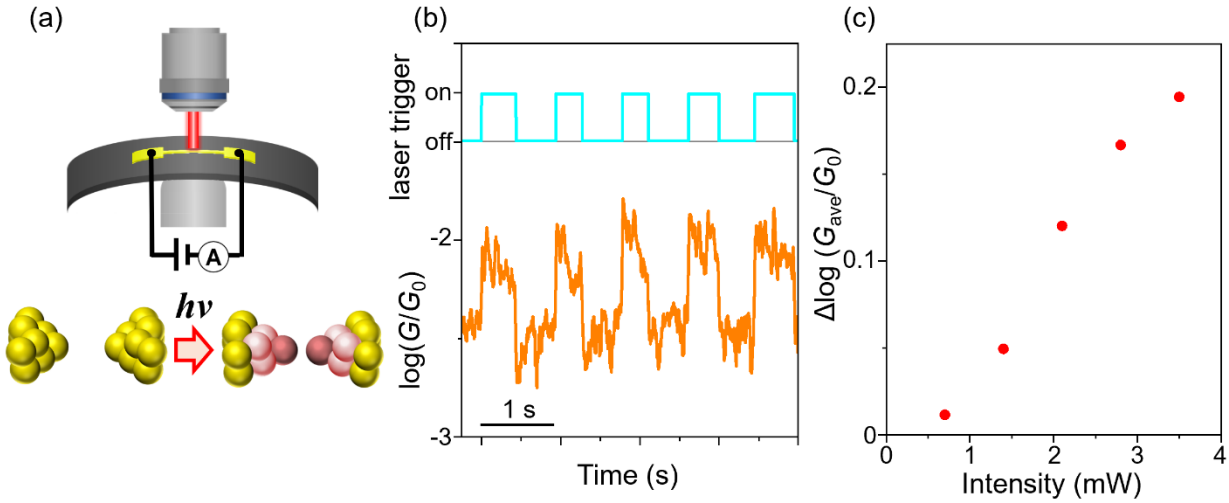

Figure 1. Au optical atomic switch. (a) Schematic of the atomic switch fabrication using the MCBJ technique. (b) Optical response of the Au atomic switch. The orange curves represent logarithm of the conductance (log(*G*/G_0)). The red curve represents trigger signal for laser operation. The laser power was 2.1 mW (67

mW/cm^2). Wavelength was 785 nm. (c) Variation of the conductance increment ($\Delta\log(G_{ave}/G_0)$) with laser intensity. The increment was calculated by subtracting the average conductance during the light ON and OFF states.

Results and discussion

Single-atom and single-molecule junctions were fabricated using the mechanically controllable break junction (MCBJ) technique (Figure 1a).[23-26] The electrode separation was precisely tuned by bending the substrate via elongation of a piezoelectric element, allowing sub-angstrom control. Conductance of the Au nanogap was modulated by adjusting the applied bias voltage. A focused 785-nm laser was irradiated onto the nanogap, resulting in a conductance increase during illumination, which returned to its original state upon cessation of irradiation (Figure 1b). The conductance switched to the value when the irradiation was stopped. To examine the relationship between optical response and laser power, the conductance increment was quantified as $\Delta\log(G_{ave}/G_0)$, where G_{ave} is the average conductance and G_0 is the quantum of conductance, represented by $2e^2/h$, e is the elementary charge, and h is Planck's constant. $\Delta\log(G_{ave}/G_0)$ was calculated by subtracting $\log(G_{ave\_ON}/G_0)$, the conductance with laser irradiation in log scale, from $\log(G_{ave\_OFF}/G_0)$, the conductance without laser irradiation in logscale. The increment increased with laser power (Figure 1 c), consistent with atomic motion induced by local plasmonic heating.[3] At the Au nanogap, LSPR generates a strong electromagnetic field at the electrode surface, raising the local temperature. This thermal activation of atomic motion narrows the nanogap, thereby increasing conductance.

Next, C_{60} molecules were introduced into the Au nanogap. Continuous optical switching was demonstrated using the C_{60} SMJ. The conductance as a function of electrode separation is shown in Figure 2(a). As the Au electrodes were gradually pulled apart, the narrowing of the contact region led to the formation of a single-atom contact. Further displacement caused the electrodes to separate, allowing a diffusing C_{60} molecule to bridge the gap. A conductance plateau at 1 G_0 corresponds to the single-atom Au contact. In the 2D conductance–displacement histogram, significant counts at larger displacements beyond the atomic contact indicate the formation of metastable SMJs. Two distinct conductance features were observed: $10^{-2.7}$ G_0 and $10^{-0.4}$ G_0 (Figure 2b). The former is consistent with previously reported values for C_{60} SMJs exhibiting strong Au–C_{60} coupling.[27, 28] The latter, higher conductance state is attributed to metal atomic contacts modulated by C_{60} adsorption.[29-32]

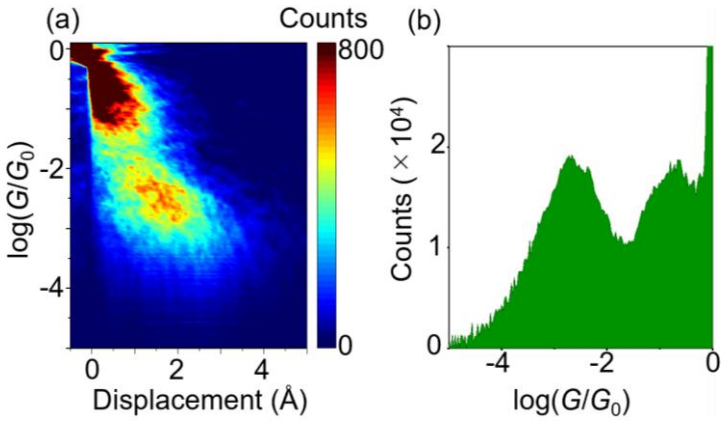

Figure 2. (a) 2D histogram of the conductance (log(G/G_0)) as a function of electrode displacement during the formation of the Au–C_{60} junction. The origin of displacement is defined at the point where the conductance reaches 1 G_0. The histogram uses 200 and 300 bins for displacement and conductance, respectively. (b) Conductance histogram of the C_{60} molecular junction plotted on the logarithmic scale. The bin size is 0.027, with a total of 1614 traces recorded under an applied bias voltage of 100 mV.

Based on the conductance–displacement analysis, we demonstrated optical switching in the C_{60} SMJ while measuring the *I–V* response. The *I–V* response provide the electronic states of the SMJs (Figure 3a).[25, 28, 33] The *I–V* curves exhibited nonlinear behavior, indicative of electron tunneling across the Au electrodes bridged by the C_{60} molecule (Figure 3a, 3b).[25, 28, 33] This nonlinearity was analyzed using a single-level transport model, in which the lowest unoccupied molecular orbital (LUMO) of C_{60} plays the dominant role in electron transmission.[25, 27, 28, 33] In the single-level model, electron transport is governed by the energy alignment of the molecular orbital (ε) relative to the Fermi level (E_F) and the coupling energy (Γ) between the molecular orbital and the metal electronic states.[25, 28, 33] The coupling energy Γ reflects the broadening of the molecular level due to hybridization (Figure 3a). Fitting the *I–V* curves yielded key parameters describing the electronic structure of the molecular junction (Figure 3b). The separation between the electrodes was adjusted using laser irradiation to achieve the conductance characteristic of the SMJ. The optical response was measured at incremental laser intensities to examine conductance modulation. At each intensity step, the *I–V* characteristics were recorded to evaluate changes in the electronic states. Analysis of the optical response revealed that conductance and Γ increased with laser intensity while ε remained constant (see Figures 3c–3f). The observed conductance values and parameters agreed with those of C_{60} molecular junctions.[27] The modulation of Γ by photoirradiation remains within the range of the deviation of the high conductivity state of the C_{60} molecular junction.[27] A 2D histogram of laser power versus conductance increment confirmed a monotonic increase in conductance with increasing laser power. The conductance enhancement induced by laser irradiation was comparable to that observed in bare Au nanogaps, suggesting that the atomic motion was also induced by local heating via LSPR, as well as the case without a C_{60} molecule. This is consistent with previous optical response molecules on metal surfaces, where photocurrent contributions were negligible due to rapid excited-state relaxation into the electrodes.[34-36] The laser power dependence of Γ and ε further supports this mechanism: Γ increased with laser power, while ε remained unchanged, indicating that the modulation arises from changes in Au–C_{60} coupling rather than shifts in molecular orbital energy. According to the continuous *I–V* measurement in the breaking process of the molecular junction, the Γ tends to decay more immediately than ε.[37]

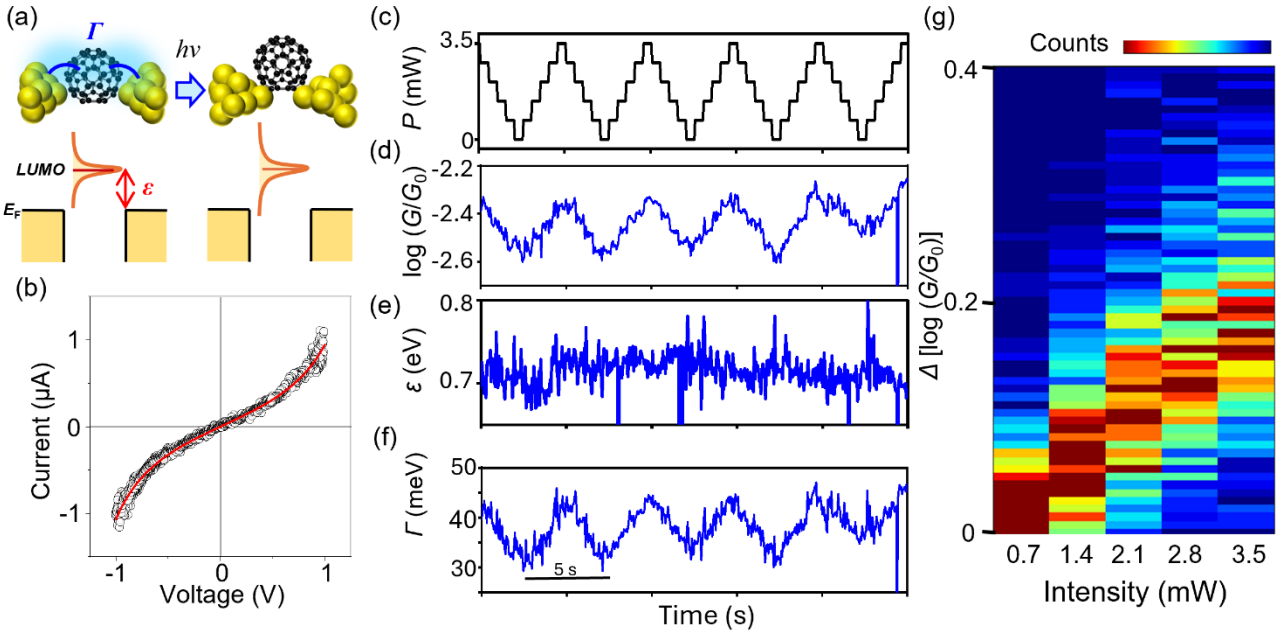

Figure 3. (a) Schematic of the change in electronic states induced by optical switching. (b) Current–voltage (*I*–*V*) characteristic curve of the C_{60} junction with a conductance of 7.3 mG_0. The red curve illustrates the fitting using the single-level model. The values of Γ and ε are 64 meV and 0.75 eV, respectively. (c–f) Optical response of the C_{60} molecular junction. (c) Laser power (*P*) vs. time. (d) Conductance in the logarithmic scale (log (G/G_0)) vs. time. Wavelength was 785 nm. (e) Relative energy of ε vs. time. (f) Γ vs. times. (The *I*–*V* curve was obtained every 1 s; the constant bias voltage was 100 mV). (g) Increase in conductance (Δlog (G_{ave}/G_0)) vs. laser power intensity (the bin sizes used were 0.7 and 0.0067).

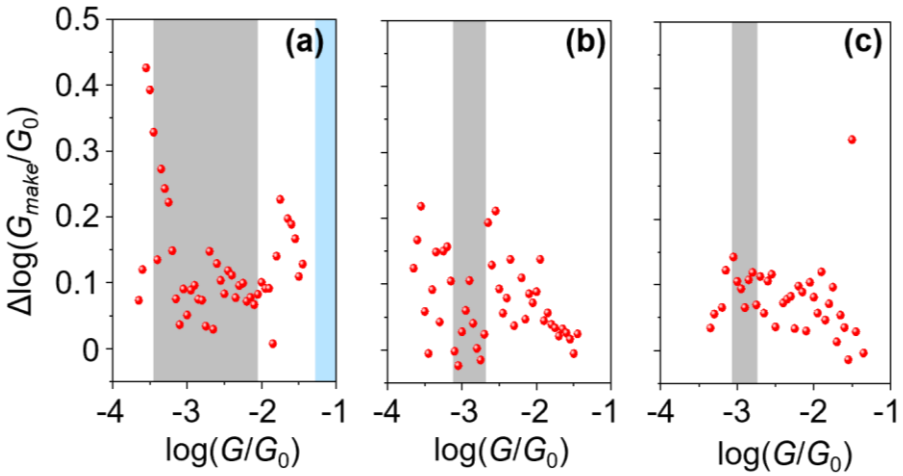

Figure 4. Relationship between the increase in conductance ($\Delta\log(G_{ave}/G_0)$) caused by laser irradiation and the initial conductance ($\log(G_{ave}/G_0)$) in the (a) C_{60}, (b) BPY, and (c) BDA junctions. Laser power is 2.1 mW.

Thus, photoinduced atomic motion reduces the Au–C_{60} separation, enhances orbital overlap, and increases the conductance of the C_{60} molecular junction. The *I–V* response represents that the C_{60} remains trapped in the Au nanogap during the laser irradiation, while the Au–C_{60} interaction was modulated by the laser irradiation. The aforementioned discussion indicates that optical irradiation induces a structural change in SMJs, thereby enabling control over their conductance.

As shown in Figure 4, $\Delta\log(G_{ave}/G_0)$ is suppressed within the conductance range characteristic of C_{60} and BPY junctions. In contrast, BDA exhibits minimal dependence of $\Delta\log(G_{ave}/G_0)$ on initial conductance. This behavior can be attributed to differences in molecular backbone stiffness and binding interactions. Regarding the backbone, saturated molecules like BDA, which contain freely rotating single bonds, have lower conformational rigidity and smaller energy barriers compared to the more rigid π-conjugated BPY and C_{60} structures.[38] Thus, $\Delta\log(G_{ave}/G_0)$ did not depend on the initial conductance for BDA junction. Regarding the interaction, electrode-C_{60}, -BPY, -BDA interactions can be represented, π, π+σ, and σ interactions.[27] Notably, $\Delta\log(G_{ave}/G_0)$ was enhanced in the high-conductance region (10^{-2}–10^{-1} G_0) of C_{60} junction, which may be attributed to the molecular bearing effect of π-conjugated systems. The delocalized π orbitals of C_{60} facilitate sliding or rotational motion on the electrode surface.[39-41] These results further support the interpretation that conductance-dependent optical response is governed by molecular stiffness and the strength of molecule–

electrode interactions.

The optical atomic switching behavior of the C_{60} molecular junction was subsequently demonstrated (Figure 5). The conductance of the SMJ responded in synchrony with the applied optical signal (Figure 5a), exhibiting stable and repeatable switching for at least 50 cycles (Figure 5b). The conductance of the ON and OFF state is $10^{-2.6\pm0.1}$ and $10^{-3.5\pm0.2}$ G_0, respectively. The optical switch response with the other frequencies was also examined (Supporting Information Figure S2). The optical switch was demonstrated for another junction, and the switch was demonstrated with a frequency of 20 Hz (Figure 5c). The deformation from the ideal square derives from the limitation of the bandwidth of the noise filter of the current amplifier. It is noticeable that the conductance value responses in the scales of sub-milliseconds, which is faster than previous optical atomic switches[3], where a 1-2 s delay was observed. Considering the thermal diffusivity of gold is estimated to be 1.27×10^{-4} m^2/s[42], the heat at the relevant area induced by the local heating effect immediately diffuses to the bulk electrode, indicating that the switching speed is governed by the response atomic motion of the junction. The optical switching of the molecular junction is regulated by the orbital coupling between the molecular orbital and the metal electronic state, as mentioned in the previous section. Because the electronic coupling is much sensitive to the junction structure, such as molecule orientation or adsorption site, the optical atomic switch of molecular junction is considered to respond more sensitively to the atomic motions. Regarding the stability of the switching, lithographically defined structure provided mechanical stability and effectively suppressed thermal drift.[15, 23, 24] Additionally, the presence of C_{60} was found to reduce surface energy, enhancing the durability of the metal–molecule contact. The ON/OFF ratio was particularly improved in the high-conductance regime.

Thus, photoinduced atomic motion reduces the Au–C_{60} separation, enhances orbital overlap, and increases the conductance of the C_{60} molecular junction. The *I–V* response represents that the C_{60} remains trapped in the Au nanogap during the laser irradiation, while the Au–C_{60} interaction was modulated by the laser irradiation. The aforementioned discussion indicates that optical irradiation induces a structural change in SMJs, thereby enabling control over their conductance.

As shown in Figure 4, $\Delta\log(G_{ave}/G_0)$ is suppressed within the conductance range characteristic of C_{60} and BPY junctions. In contrast, BDA exhibits minimal dependence of $\Delta\log(G_{ave}/G_0)$ on initial conductance. This

behavior can be attributed to differences in molecular backbone stiffness and binding interactions. Regarding the backbone, saturated molecules like BDA, which contain freely rotating single bonds, have lower conformational rigidity and smaller energy barriers compared to the more rigid π-conjugated BPY and C_{60} structures.[38] Thus, $\Delta\log(G_{ave}/G_0)$ did not depend on the initial conductance for BDA junction. Regarding the interaction, electrode-C_{60}, -BPY, -BDA interactions can be represented, π, π+σ, and σ interactions.[27] Notably, $\Delta\log(G_{ave}/G_0)$ was enhanced in the high-conductance region (10^{-2}–10^{-1} G_0) of C_{60} junction, which may be attributed to the molecular bearing effect of π-conjugated systems. The delocalized π orbitals of C_{60} facilitate sliding or rotational motion on the electrode surface.[39-41] These results further support the interpretation that conductance-dependent optical response is governed by molecular stiffness and the strength of molecule–electrode interactions.

The optical atomic switching behavior of the C_{60} molecular junction was subsequently demonstrated (Figure 5). The conductance of the SMJ responded in synchrony with the applied optical signal (Figure 5a), exhibiting stable and repeatable switching for at least 50 cycles (Figure 5b). The conductance of the ON and OFF state is $10^{-2.6\pm0.1}$ and $10^{-3.5\pm0.2}$ G_0, respectively. The optical switch response with the other frequencies was also examined (Supporting Information Figure S2). The optical switch was demonstrated for another junction, and the switch was demonstrated with a frequency of 20 Hz (Figure 5c). The deformation from the ideal square derives from the limitation of the bandwidth of the noise filter of the current amplifier. It is noticeable that the conductance value responses in the scales of sub-milliseconds, which is faster than previous optical atomic switches[3], where a 1-2 s delay was observed. Considering the thermal diffusivity of gold is estimated to be 1.27×10^{-4} m^2/s[42], the heat at the relevant area induced by the local heating effect immediately diffuses to the bulk electrode, indicating that the switching speed is governed by the response atomic motion of the junction. The optical switching of the molecular junction is regulated by the orbital coupling between the molecular orbital and the metal electronic state, as mentioned in the previous section. Because the electronic coupling is much sensitive to the junction structure, such as molecule orientation or adsorption site, the optical atomic switch of molecular junction is considered to respond more sensitively to the atomic motions. Regarding the stability of the switching, lithographically defined structure provided mechanical stability and effectively suppressed thermal drift.[15, 23, 24] Additionally, the presence of C_{60} was found to reduce surface energy, enhancing the durability of the metal–molecule contact. The ON/OFF ratio was particularly improved in the

high-conductance regime.

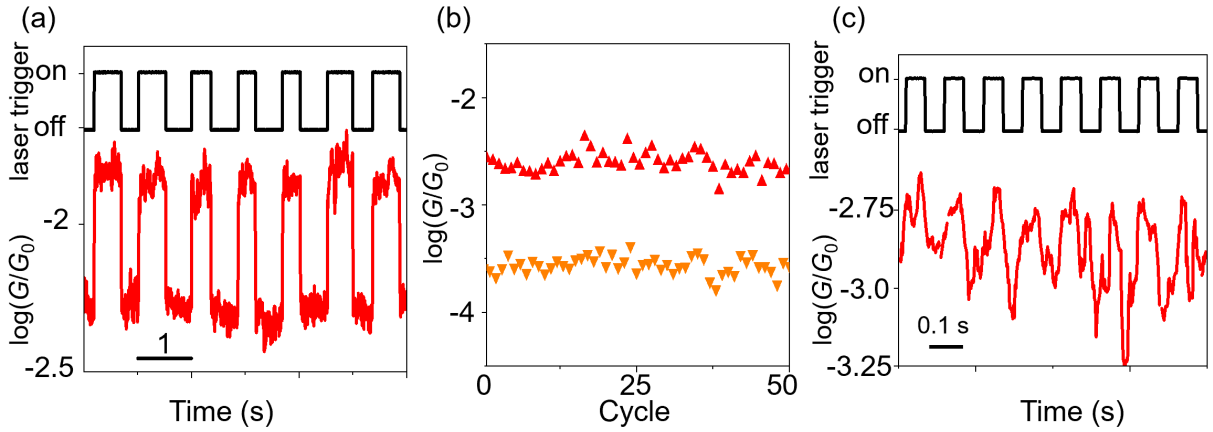

Figure 5. (a) Optical switch of the C_{60} molecular junction operating at a frequency of 1 Hz. (b) Continuous operation of the optical switch. The conductance of ON/OFF state was $10^{-2.6\pm0.1}/10^{-3.5\pm0.2}$ G_0. (c) Optical switch of the C_{60} molecular junction operating at a frequency of 20 Hz. The laser power was 2.1 mW.

Conclusions

In this study, we demonstrated optical atomic switching by precisely controlling the electrode separation in Au nanogap junctions and investigated the molecular influence on conductance modulation. Conductance–displacement analysis confirmed the formation of C_{60}-based SMJs. *I–V* characterization under photoirradiation revealed that atomic motion modulates the Au–C_{60} distance, enhancing conductance via increased metal–molecule coupling. A systematic investigation of conductance enhancement as a function of initial conductance highlighted the roles of molecular stiffness and electrode–molecule interactions. Flexible molecules like BDA exhibited conductance responses independent of their initial state, whereas rigid, π-conjugated molecules such as C_{60} facilitated more durable atomic contacts and greater conductance enhancement under irradiation.

Methods

Au atomic contacts and molecular junctions were fabricated an MCBJ setup at 300K (Figure 1a). The MCBJ samples were prepared using standard nanofabrication techniques, as detailed in the Supporting Information. Briefly, a polyimide film was deposited onto a phosphor bronze substrate coated with a 1-μm insulating SiO_2 layer. Au nanoelectrodes were patterned on the polyimide-coated surface via electron beam

lithography. The underlying polyimide was then removed by isotropic reactive ion etching, resulting in a free-standing Au nanobridge (ca. 1 μm in length) suspended over the substrate. To introduce C_{60} molecules, a 500-μM toluene solution was drop-cast onto the unbroken Au nanobridge. For the introduction of BPY and BDA, we used ethanol solution. The concentration was 300 μM and 500 μM for BPY and BDA. Mechanical breaking of the bridge was achieved by bending the substrate using the MCBJ setup, thereby forming single-atom or single-molecule junctions.

A 785-nm optical laser was focused onto the junction using a ×50 objective lens. Laser timing was controlled by a digital signal processing system. Detailed measurement protocols are provided in the Supplementary Information.

Author contributions

All authors contributed equally to this manuscript and approved its final version.

Conflicts of interest

There are no conflicts of interest to declare.

Data availability

Data for this article, including csv files are available at figshare at 10.6084/m9.figshare.30399460.

Acknowledgments

This work was partially supported by the Yazaki Memorial Foundation for Science and Technology, Murata Science and Education Foundation, and JSPS KAKENHI (Grant Number 25K01740).

References

1. PsiQuantum Team, *Nature*, 2025, **641**, 876-883.
2. A. Emboras, J. Niegemann, P. Ma, C. Haffner, A. Pedersen, M. Luisier, C. Hafner, T. Schimmel and J. Leuthold, *Nano Lett.*, 2016, **16**, 709-714.
3. W. Zhang, H. Liu, J. Lu, L. Ni, H. Liu, Q. Li, M. Qiu, B. Xu, T. Lee, Z. Zhao, X. Wang, M. Wang, T. Wang, A. Offenhausser, D. Mayer, W. T. Hwang and D. Xiang, *Light. Sci. Appl.*, 2019, **8**, 34.

4. H. Zhang, J. Li, C. Yang and X. Guo, *Acc. Mater. Res.*, 2024, **5**, 971-986.
5. P. S. Peercy, *Nature*, 2000, **406**, 1023-1026.
6. T. G. Tiecke, J. D. Thompson, N. P. de Leon, L. R. Liu, V. Vuletic and M. D. Lukin, *Nature*, 2014, **508**, 241-244.
7. J. P. Covey, H. Weinfurter and H. Bernien, *Npj Quantum Inf.*, 2023, **9**, 90.
8. H. Huang, S. Shi, J. Zha, Y. Xia, H. Wang, P. Yang, L. Zheng, S. Xu, W. Wang, Y. Ren, Y. Wang, Y. Chen, H. P. Chan, J. C. Ho, Y. Chai, Z. Wang and C. Tan, *Nat. Commun.*, 2025, **16**, 3836.
9. H. Lin, J. Ou, Z. Fan, X. Yan, W. Hu, B. Cui, J. Xu, W. Li, Z. Chen, B. Yang, K. Liu, L. Mo, M. Li, X. Lu, G. Zhou, X. Gao and J. M. Liu, *Nat. Commun.*, 2025, **16**, 421.
10. A. Ashkin, *Phys. Rev. Lett.*, 1970, **24**, 156-159.
11. A. Ashkin and J. M. Dziedzic, *Science*, 1987, **235**, 1517-1520.
12. I. Heller, T. P. Hoekstra, G. A. King, E. J. Peterman and G. J. Wuite, *Chem. Rev.*, 2014, **114**, 3087-3119.
13. Y. Zhang, C. Min, X. Dou, X. Wang, H. P. Urbach, M. G. Somekh and X. Yuan, *Light. Sci. Appl.*, 2021, **10**, 59.
14. T. Shoji and Y. Tsuboi, *J. Phys. Chem. Lett.*, 2014, **5**, 2957-2967.
15. F. Evers, R. Korytár, S. Tewari and J. M. van Ruitenbeek, *Rev. Mod. Phys.*, 2020, **92**, 035001.
16. X. Xie, P. Li, Y. Xu, L. Zhou, Y. Yan, L. Xie, C. Jia and X. Guo, *ACS Nano*, 2022, **16**, 3476-3505.
17. A. K. Mitchell, K. G. L. Pedersen, P. Hedegard and J. Paaske, *Nat. Commun.*, 2017, **8**, 15210.
18. Z. Chen, I. M. Grace, S. L. Woltering, L. Chen, A. Gee, J. Baugh, G. A. D. Briggs, L. Bogani, J. A. Mol, C. J. Lambert, H. L. Anderson and J. O. Thomas, *Nat. Nanotechnol.*, 2024, **19**, 986-992.
19. Y. Zheng, P. Duan, Y. Zhou, C. Li, D. Zhou, Y. Wang, L. C. Chen, Z. Zhu, X. Li, J. Bai, K. Qu, T. Gao, J. Shi, J. Liu, Q. C. Zhang, Z. N. Chen and W. Hong, *Angew. Chem. Int. Ed. Engl.*, 2022, **61**, e202210097.
20. H. Yin, H. Lin, Y. Zong and X.-D. Wang, *Org. Electron.*, 2021, **93**.
21. M. Takei, M. Takeuchi, H. Suga, T. Wakahara, K. Wakabayashi, S. Okada and K. Tsukagoshi, *ACS Appl. Electron. Mater.*, 2023, **5**, 3184-3189.
22. E. Gorenskaia and P. J. Low, *Chem Sci*, 2024, **15**, 9510-9556.
23. C. A. Martin, D. Ding, H. S. J. van der Zant and J. M. van Ruitenbeek, *New J. Phys.*, 2008, **10**, 065008.
24. J. M. van Ruitenbeek, A. Alvarez, I. Piñeyro, C. Grahmann, P. Joyez, M. H. Devoret, D. Esteve and C. Urbina, *Rev. Sci. Instrum.*, 1996, **67**, 108-111.
25. S. Kaneko, D. Murai, S. Marques-Gonzalez, H. Nakamura, Y. Komoto, S. Fujii, T. Nishino, K. Ikeda, K. Tsukagoshi and M. Kiguchi, *J. Am. Chem. Soc.*, 2016, **138**, 1294-1300.
26. M. Ichikawa, K. Tsukagoshi, T. Nishino and S. Kaneko, *ACS Appl. Nano Mater.*, 2025, **8**, 13620-13627.

27. Y. Isshiki, S. Fujii, T. Nishino and M. Kiguchi, *J. Am. Chem. Soc.*, 2018, **140**, 3760-3767.
28. K. Yasuraoka, S. Kaneko, S. Kobayashi, K. Tsukagoshi and T. Nishino, *ACS Appl. Mater. Interfaces*, 2021, **13**, 51602-51607.
29. C. Z. Li, H. X. He, A. Bogozi, J. S. Bunch and N. J. Tao, *Appl. Phys. Lett.*, 2000, **76**, 1333-1335.
30. H. Häkkinen, R. N. Barnett and U. Landman, *J. Phys. Chem. B*, 1999, **103**, 8814-8816.
31. R. Fukuzumi, S. Kaneko, S. Fujii, T. Nishino and M. Kiguchi, *ChemPhysChem*, 2020, **21**, 175-180.
32. S. Kaneko, Y. Nakamura, J. Zhang, X. Yang, J. Zhao and M. Kiguchi, *J. Phys. Chem. C*, 2014, **119**, 862-866.
33. Y. Kim, T. Pietsch, A. Erbe, W. Belzig and E. Scheer, *Nano Lett.*, 2011, **11**, 3734-3738.
34. M. Vadai, N. Nachman, M. Ben-Zion, M. Bürkle, F. Pauly, J. C. Cuevas and Y. Selzer, *J. Phys. Chem. Lett.*, 2013, **4**, 2811-2816.
35. C. Boerigter, U. Aslam and S. Linic, *ACS Nano*, 2016, **10**, 6108-6115.
36. Y. Zhang, Y. Luo, Y. Zhang, Y. J. Yu, Y. M. Kuang, L. Zhang, Q. S. Meng, Y. Luo, J. L. Yang, Z. C. Dong and J. G. Hou, *Nature*, 2016, **531**, 623-627.
37. Y. Isshiki, E. Montes, T. Nishino, H. Vazquez and S. Fujii, *Chem. Sci.*, 2024, **15**, 17328-17336.
38. A. S. Gilbert, *Thermochim. Acta*, 1999, **339**, 131-142.
39. N. Neel, J. Kroger and R. Berndt, *Nano Lett.*, 2011, **11**, 3593-3596.
40. D. V. Gruznev, A. V. Matetskiy, L. V. Bondarenko, A. V. Zotov, A. A. Saranin, J. P. Chou, C. M. Wei and Y. L. Wang, *Surf. Sci.,* 2013, **612**, 31-36.
41. H. Shin, A. Schwarze, R. D. Diehl, K. Pussi, A. Colombier, É. Gaudry, J. Ledieu, G. M. McGuirk, L. N. Serkovic Loli, V. Fournée, L. L. Wang, G. Schull and R. Berndt, *Phys. Rev. B*, 2014, **89**, 245428.
42. F. Kreith and W. Z. Blackie, *Basic Heat Transfer*, Harper and Row Publishers, New York, 1980.